Available online at www.sciencedirect.com
ScienceDirect
Journal of Nuclear Materials 362 (2007) 116–127
journal of nuclear materials
www.elsevier.com/locate/jnucmat

The development of radiation embrittlement models for US power reactor pressure vessel steels

J.A. Wang *, N.S.V. Rao, S. Konduri

Oak Ridge National Laboratory, 1 Bethel Valley Road, Oak Ridge, TN 37831, United States

Received 6 January 2005; accepted 7 November 2006

Abstract

A new approach of utilizing information fusion technique is developed to predict the radiation embrittlement of reactor pressure vessel steels. The Charpy transition temperature shift data contained in the Power Reactor Embrittlement Database is used in this study. Six parameters-Cu, Ni, P, neutron fluence, irradiation time, and irradiation temperature – are used in the embrittlement prediction models. The results indicate that this new embrittlement predictor achieved reductions of about 49.5% and 52% in the uncertainties for plate and weld data, respectively, for pressurized water reactor and boiling water reactor data, compared with the Nuclear Regulatory Commission Regulatory Guide 1.99, Rev. 2. The implications of dose-rate effect and irradiation temperature effects for the development of radiation embrittlement models are also discussed.
© 2006 Elsevier B.V. All rights reserved.

1. Introduction

The application of the information fusion technique to RPV radiation embrittlement was first developed by the authors [1]. In this earlier work, general electric boiling water reactor (BWR) RPV surveillance data consisting of 112 RPV surveillance data points from RPV base and weld materials were used to develop embrittlement models. For this data, the information fusion approach achieved about 56% and 62% reductions in uncertainties for base and weld materials, respectively, compared to the prediction of the Nuclear Regulatory Commission's (NRC's) Regulatory Guide 1.99, Rev. 2.

Currently, based on the ASTM E10.02 database and the Oak Ridge National Laboratory (ORNL) Power Reactor Embrittlement Database (PR-EDB) [2,3], about 900 RPV surveillance transition temperature shift data points are available for base and weld materials from the US Power Reactor Surveillance Program. Despite the demonstrated effectiveness of the information fusion technique in predicting RPV embrittlement in BWR data [1], its scope is somewhat limited, since these BWR data constitute only a relatively small portion of the overall RPV surveillance data. Thus, further verification of the general applicability of the information fusion technique to determining the radiation

* Corresponding author. Fax: +1 865 574 2274.
E-mail address: wangja@ornl.gov (J.A. Wang).

0022-3115/$ - see front matter © 2006 Elsevier B.V. All rights reserved.
doi:10.1016/j.jnucmat.2006.12.013

embrittlement of RPV steels is needed. Verification is the main focus of the present study.

2. New approach for evaluating radiation embrittlement

2.1. Information fusion approach

The complex nonlinear dependencies observed in typical RPV material embrittlement data, as well as the inherent large uncertainties and scatter in the data, make prediction of radiation embrittlement a difficult task. Conventional statistical and deterministic approaches have only resulted in rather large uncertainties, in part because they do not fully exploit domain-specific mechanisms. The mechanism models built by researchers in the field, on the other hand, do not fully exploit the statistical and information content of the data. As evidenced in previous studies, it is unlikely that a *single* method, whether statistical, nonlinear, or mechanism model, will outperform all others. In this paper, we combined a number of complementary methods including mechanism models, neural networks, and nearest-neighbor regressions (NNRs). Such a combination of methods has become possible because of recent developments in measurement-based optimal fusers [4–6] in the area of information fusion. The isolation fusers [7] was used to combine various methods, which guarantees to be at least as good, according to a chosen criterion such as prediction error, as the best individual estimator with a specified probability. Informally, the isolation property ensures that the fuser is at least capable of simply 'imitating' any of the models, but in general it can perform and does much better in practice. This result is distribution-free in that no assumptions are made on the underlying error distributions. More recently, projective fusers have been developed [8]. These fusers, based on choosing the models with minimum localized error, offer stronger guarantees that fusion of no proper subset of the models performs better than the fused system based on all models. Thus, the positive aspects of *all* individual estimators can be exploited without discarding any single estimator. The deployment of these fusers on various models will ensure (probabilistically) that the fused model is at least as good as the best of the individual models, irrespective of their individual performances. In practice, however, because of the general nature of the results on fusers, the actual performance gains in a particular application are often better than the analytical guarantees. Typically, the required sample size is much smaller (but never larger) than the predicted sample size. We show here that significant performance improvements are indeed obtained by employing fusers to combine various embrittlement models.

2.2. Methodology used for developing embrittlement models

Firstly, several improved embrittlement models, based on PR-EDB and utilizing the copper precipitation and matrix damage mechanism theory, were developed. We then employ neural networks, NNRs, and other mechanism models, based on the PR-EDB data, to predict the Charpy transition temperature shift (ΔT_{30}) of RPV materials.

The first task is to create unbiased training and test sets. The RPV surveillance data (listed in the ASTM E10.02 database and PR-EDB) is preprocessed and streamlined, and data values are then scaled to the interval $[-1, 1]$ using a linear max/min transformation. This ensures that no one component in the data dominates the parameter optimization scheme. Then the data are randomly partitioned into training and testing sets. Three groups of the sample data are used for model development as described below:

- The PWR data (746 samples), including (a) 518 base data points where 468 data points were used as training set and 50 data points were used as a testing set, and (b) 228 weld data where 208 data points were used as a training set and 20 data points were used as a testing set.
- The BWR data (152 samples), including (a) 83 base data where 73 data points were used as a training set and 10 data points were used as a testing set, and (b) 69 weld data points where 60 data points were used as a training set and 9 data points were used as a testing set.
- The combined BWR and PWR data (899 samples), including (a) 601 base data points where 541 data points were used as a training set and 60 data points were used as testing set, and (b) 298 weld data points where 268 data points were used as a training set and 30 data points were used as a testing set.

The sensitivity of the sample size was not investigated in the current study.

The second task consists of determining the number of estimators for this problem. For each method, we selected a criteria function and an optimization routine that consistently produce stable results. For statistical estimators, we followed the procedure described in the literature [5,8–10]. For artificial neural networks (ANNs) [10], 1 hidden layer and 11 hidden nodes were chosen with 2000-epoch iteration. A random number generator was used to generate the initial weights for ANNs. Four sets of ANN models were tested. We then combined the statistical and deterministic estimators using information fusion techniques.

An optimal projective fuser [5] proposed earlier was based on the lower envelope of error regressions of the estimators. In most practical cases, however, error regressions are not available, and only a finite sample is given. Consequently, this fuser is hard to implement; furthermore, it provides only asymptotic consistency. In this paper, we employ a projective fuser based on the nearest-neighbor concept [8], which is easy to implement. The combined system is guaranteed in a probabilistic sense to perform at least as well as the best model even locally by exploiting the regions where the individual models are superior.

2.3. Embrittlement prediction models

In this section we briefly describe various models used for embrittlement prediction. These models are combined in the next section.

Wang–Rao–Konduri (WRK) embrittlement prediction models. The residual defects in materials due to neutron-induced displacement damage are a function of neutron energy, neutron flux, exposure temperature, and the material properties that determine how neutrons interact with atoms and how defects interact within the material [11]. Thus, temperature, neutron flux, neutron energy spectrum, material composition, and processing history all contribute to the radiation embrittlement process [12].

The development of new embrittlement prediction equations [13,14] stems from a series of studies on radiation embrittlement models, such as Guthrie's model [15], the model of Odette et al. [16], Fisher and Buswell's model [17], Lowe and Pegram's model [18], the French model [19], and several other parameter studies on the PR-EDB. Although the copper-precipitation model, in addition to the matrix damage model, has been extremely successful in explaining many aspects of irradiation embrittlement, it is becoming increasingly evident that other elements also contribute to the embrittlement of RPV steel, such as Ni, P, Mn, Mo, and S. Theoretically, all the impurities in low-alloy steel are candidates for inclusion in the modeling. For example, C, Si, Mn, Mo, S, and other elements were investigated in the test run, but including or excluding these elements did not affect the overall outcome of the statistical parameters significantly; therefore, these parameters (or elements) were not incorporated into final governing equations. Thus, Cu, Ni, and P were tentatively selected as key elements and were incorporated into the formula for the new prediction equations. Furthermore, the reasons for separating weld and base metals are because the welds tend to show enhanced degradation, the welding process presents a possible region of physical and metallurgical discontinuity, and welding offers added chances for the introduction of defects and undesirable components or stresses.

A nonlinear least-squares fitting FORTRAN program was written for this study. The governing equation of the new model is based on the copper precipitation and matrix damage models. The development of the parameters for this new embrittlement model is based on statistical formulation chosen by computer iterations. Three new prediction models each for PWR data and the combined PWR and BWR data were developed, where the 'dose rate' and 'dose rate plus irradiation temperature' effects are considered in the development of Model II and Model III, respectively, as described below.

WRK models for PWR data

Model I (baseline model without irradiation time and temperature)

$$\begin{aligned}\Delta\mathrm{RTNDT(Base)} &= (38.863 - 211.865\mathrm{P/Ni} + 1042.37\mathrm{P} \\ &\quad + 241.084(\mathrm{Cu} - 0.07) \\ &\quad + 223.972\sqrt{(\mathrm{Cu} - 0.07)\mathrm{Ni}} - 25.988\mathrm{Ni})f^{0.32-0.023\ln f}\end{aligned} \tag{1}$$

$$\begin{aligned}\Delta\mathrm{RTNDT(Weld)} &= (4.53 + 162.776\mathrm{P/Ni} - 70.151\mathrm{P} - 86.971(\mathrm{Cu} - 0.07) \\ &\quad + 488.082\sqrt{(\mathrm{Cu} - 0.07)\mathrm{Ni}} + 31.765\mathrm{Ni})f^{0.255-0.041\ln f}\end{aligned} \tag{2}$$

Model II (model with irradiation time, without irradiation temperature)

$$\begin{aligned}\Delta\text{RTNDT(Base)} &= (6.988 - 118.69\text{P/Ni} + 511.906(\text{Cu} - 0.07) \\ &\quad + 105.766\sqrt{(\text{Cu} - 0.07)\text{Ni}} + 550.289\text{P})f^{0.017-0.169\ln f} \\ &\quad + (35.764(\text{Cu} - 0.07) - 34.422\sqrt{(\text{Cu} - 0.07)\text{Ni}} - 6.142) \\ &\quad \times f(-2.256 - 0.013\ln f\ln(t_i/600\,000)) \end{aligned} \quad (3)$$

$$\begin{aligned}\Delta\text{RTNDT(Weld)} &= (13.58 + 74.623\text{P/Ni} - 132.155(\text{Cu} - 0.07) \\ &\quad + 516.216\sqrt{(\text{Cu} - 0.07)\text{Ni}} + 610.399\text{P})f^{0.188-0.084\ln f} \\ &\quad + (5.167(\text{Cu} - 0.07)\text{Ni} + 0.721) \\ &\quad \times f(-2.256 - 0.013\ln f\ln(t_i/600\,000)) \end{aligned} \quad (4)$$

Model III (model with irradiation time and temperature)

$$\begin{aligned}\Delta\text{RTNDT(Base)} &= (230.939(\text{Cu} - 0.07) + 347.024\sqrt{(\text{Cu} - 0.07)\text{Ni}} + 770.618\text{P}) \\ &\quad \times (f^{0.188-0.089\ln f})\text{TANH}[1/(31.039(T_i/1010) - 16.04)] \\ &\quad + (-4.387\sqrt{(\text{Cu} - 0.07)\text{Ni}} - 15.154\text{Ni}(\text{Cu} - 0.07) + 6.475) \\ &\quad \times f(2.086 - 0.069\ln f\ln(t_i/600\,000)) \end{aligned} \quad (5)$$

$$\begin{aligned}\Delta\text{RTNDT(Weld)} &= (153.96\text{P/Ni} - 186.36(\text{Cu} - 0.07) \\ &\quad + 668.707\sqrt{(\text{Cu} - 0.07)\text{Ni}} - 364.926\text{P})(f^{0.233-0.057\ln f})\text{TANH} \\ &\quad \times [1/(22.935(T_i/1010) - 11.71)] + (-35.659\sqrt{(\text{Cu} - 0.07)\text{Ni}} \\ &\quad + 35.2(\text{Cu} - 0.07) + 7.69\text{Ni}) \\ &\quad \times f(4.286 + 1.177\ln f\ln(t_i/600\,000)) \end{aligned} \quad (6)$$

In these models ΔRTNDT is the transition temperature shift in °F; temperature T_i is in °F; neutron fluence f is in units of 10^{19} n/cm^2 ($E > 1$ MeV); effective full power time t_i, is in hours; and Cu, Ni, and P are in wt%.

WRK Models for Combined PWR and BWR Data.

Model I (Baseline Model w/o irradiation time and temperature)

$$\begin{aligned}\Delta\text{RTNDT(Base)} &= (33.246 - 174.946\text{P/Ni} + 1356.022\text{P} + 227.318(\text{Cu} - 0.07) \\ &\quad + 223.099\sqrt{(\text{Cu} - 0.07)\text{Ni}} - 23.069\text{Ni})f^{0.296-0.008\ln f} \end{aligned} \quad (7)$$

$$\begin{aligned}\Delta\text{RTNDT(Weld)} &= (8.898 + 169.487\text{P/Ni} - 319.076\text{P} - 74.685(\text{Cu} - 0.07) \\ &\quad + 483.148\sqrt{(\text{Cu} - 0.07)\text{Ni}} + 31.045\text{Ni})f^{0.224-0.023\ln f} \end{aligned} \quad (8)$$

Model II

$$\begin{aligned}\Delta\text{RTNDT(Base)} &= (7.305 - 105.775\text{P/Ni} + 564.059(\text{Cu} - 0.07) \\ &\quad + 105.672\sqrt{(\text{Cu} - 0.07)\text{Ni}} + 913.291\text{P})f^{0.172-0.038\ln f} \\ &\quad + (72.105(\text{Cu} - 0.07) - 31.628\sqrt{(\text{Cu} - 0.07)\text{Ni}} - 5.198) \\ &\quad \times f(-2.048 - 0.004\ln f\ln(t_i/600\,000)) \end{aligned} \quad (9)$$

$$\begin{aligned}\Delta\text{RTNDT(Weld)} &= (25.286 + 79.23\text{P/Ni} - 116.417(\text{Cu} - 0.07) \\ &\quad + 513.085\sqrt{(\text{Cu} - 0.07)\text{Ni}} + 348.227\text{P})f^{0.195-0.037\ln f} \\ &\quad + (1.344(\text{Cu} - 0.07)\text{Ni} + 0.944) \\ &\quad \times f(-4.57 - 2.002\ln f\ln(t_i/600\,000)) \end{aligned} \quad (10)$$

Model III

$$\begin{aligned}\Delta\text{RTNDT(Base)} &= (202.542(\text{Cu} - 0.07) + 388.389\sqrt{(\text{Cu} - 0.07)\text{Ni}} + 1113.706\text{P}) \\ &\quad \times (f^{0.289-0.021\ln f})\text{TANH}[1/(16.989(T_i/1010) - 16.121)] \\ &\quad + (-26.457\sqrt{(\text{Cu} - 0.07)\text{Ni}} - 5.209\text{Ni}(\text{Cu} - 0.07) + 5.614) \\ &\quad \times f(2.11 - 0.073\ln f\ln(t_i/600\,000)) \end{aligned} \quad (11)$$

$$\begin{aligned}\Delta\text{RTNDT(Weld)} &= (165.874\text{P/Ni} - 147.611(\text{Cu} - 0.07) + 663.656\sqrt{(\text{Cu} - 0.07)\text{Ni}} \\ &\quad - 342.643\text{P})(f^{0.215-0.04\ln f})\text{TANH}[1/(11.549(T_i/1010) - 10.69)] \\ &\quad + (-33.156\sqrt{(\text{Cu} - 0.07)\text{Ni}} + 31.972(\text{Cu} - 0.07) + 7.802\text{Ni}) \\ &\quad \times f(4.631 + 1.334\ln f\ln(t_i/600\,000)) \end{aligned} \quad (12)$$

WRK Models for BWR Data

Two new prediction models for the GE BWR data were also developed. Irradiation time and irradiation temperature were considered in Model II. Only the irradiation time was considered in Model I, as described below.

Model I:

$$\begin{aligned}\Delta\text{RTNDT(Base)} &= (9.987 + 267.018\text{Cu} - 1.857\sqrt{\text{CuNi}} - 133.674\text{P/Cu}) \\ &\quad \times f^{-0.381-0.124\ln f} + (7.382 - 21.645\sqrt{\text{CuNi}} - 1.562\text{Cu} \\ &\quad - 37.011\text{P/Cu})f(-26.703 - 2.19\ln f \times \ln(t_i/600\,000)) \end{aligned} \quad (13)$$

$$\begin{aligned}\Delta\text{RTNDT(Weld)} &= 0.565(440.195\text{Cu} + 261.083\sqrt{\text{CuNi}} - 13.387\text{P/Cu}) \\ &\quad \times f^{-0.434-0.212\ln f} + 0.476(5.231\text{Ni} + 9.78\text{Cu}) \\ &\quad \times f(16.623 - 1.449\ln f\ln(t_i/600\,000)) \end{aligned} \quad (14)$$

Model II:

$$\begin{aligned}\Delta\text{RTNDT(Base)} &= (80.702\text{Cu} + 2.719\text{Ni} - 32.476\text{P/Cu}) \\ &\quad \times (f^{-0.004155-0.068\ln f})(e^{\frac{103.588}{T_i-473.576}}) \\ &\quad + (-11.218 + 7.827\text{Ni} + 32.149\text{Cu} + 60.406\text{P/Cu}) \\ &\quad \times f(14.315 + 1.2\ln f\ln(t_i/600\,000)) \end{aligned} \quad (15)$$

$$\begin{aligned}\Delta\text{RTNDT(Weld)} &= (627.252\text{Cu} - 23.165P/\text{Cu})(f^{0.259-0.055\ln f}) \\ &\quad \times (e^{\frac{2.542}{T_i-525.237}}) + 2.832(6.142\text{Ni} - 17.183\text{Cu}) \\ &\quad \times f(5.859 + 1.449\ln f\ln(t_i/600\,000)) \end{aligned} \quad (16)$$

Table 1
Two-sigma uncertainty bound of residual for WRK Fuser Model I and the RG1.99/R2's model

Data type	Residual uncertainty °C (°F)				Reduction in uncertainty from Fuser Model I (%)	
	RG 1.99/R2 Model		WRK Fuser Model I			
	Base	Weld	Base	Weld	Base	Weld
BWR	27.5(49.6)	33.0(59.4)	13.0(23.4)	18.8(33.9)	52.8	33.9
PWR	26.7(48.2)	33.8(60.8)	19.1(34.4)	22.3(40.2)	28.6	33.9
BWR + PWR	27.0(48.6)	34.9(62.8)	18.2(32.7)	22.7(40.9)	32.7	34.9

Table 2
Weights of linear fuser used for WRK Fuser Model I

Data type	Material	Model							
		ANN1	ANN2	ANN3	ANN4	WRK1	WRK2	Eason	K-NNR
BWR	Base	0.093	0.194	−3.210	2.801	0.465	0.286	−0.231	0.592
	Weld	−0.046	0.181	0.018	0.253	−0.045	0.381	0.051	0.603
PWR	Base	−0.07	0.089	0.043	0.001	−0.301	0.614	−0.149	0.846
	Weld	0.037	0.012	−0.049	−0.051	−0.193	0.507	0.088	0.682
BWR + PWR	Base	0.058	−0.055	0.032	−0.012	−0.244	0.460	−0.116	0.922
	Weld	−1.658	−0.928	0.736	1.798	−0.170	0.438	0.079	0.685

Regulatory Guide 1.99, Rev. 2 (RG1.99/R2) model. The transition temperature shift of the RG1.99/R2 model [20] was also used in this study for comparison. It is described as

$$\Delta RT_{NDT} = (CF) f^{(0.28-0.10\log f)}, \tag{17}$$

where ΔRT_{NDT} is the transition temperature shift in °F; CF(°F) is the chemistry factor (given in Tables 1 and 2 of RG1.99/R2), which is a function of Cu and Ni content; and neutron fluence f is in units of 10^{19} n/cm^2 ($E > 1$ MeV).

Eason's models. The embrittlement model developed by Eason et al. (Eason's model) [21] was used in this study. Development of Eason's trend curve of transition temperature shift was based on power reactor data and is described in Eq. (18).

$$\begin{aligned}
&\Delta T_{30p} = ff_1(\phi t) + ff_2(\phi t) * f(cc), \quad [^\circ F] \\
&ff_1(\phi t) = A * \exp\left[\frac{1.906\times 10^4}{T_c + 460}\right] * (1 + 57.7P) * \left[\frac{\phi t}{10^{19}}\right]^a \\
&ff_2(\phi t) = \frac{1}{2} + \frac{1}{2}\tanh\left[\frac{\log(\phi t + 5.48\times 10^{12} t_i) - 18.29}{0.600}\right] \\
&ff(cc) = B(Cu - 0.072)^{0.682}(1 + 2.56Ni^{1.358}),
\end{aligned} \tag{18}$$

where $a = 0.4449 + 0.0597 * \log(\phi t/10^{19})$, ϕt = fast neutron fluence ($E > 1$ MeV); for Welds: $A = 1.10\times 10^{-7}$, $B = 209$; for Plates: $A = 1.24\times 10^{-7}$, $B = 172$; for Forgings: $A = 0.90\times 10^{-7}$, $B = 135$; and T_c is coolant inlet temperature, °F.

ANN models. An ANN implements a parameterized nonlinear mapping from an input space to an output space [10]. A multilayer ANN (ML-ANN) is the most common architecture. The information from each input-layer node is fanned out to nodes in the hidden layer between the input and output layers. The information entering a node in any hidden or output layer is the weighted sum of all outputs in the previous layer. The node performs a nonlinear/sigmoidal transformation on the weighted sum it receives and fans out the result to all nodes in the next layer (except the output nodes). The weights are free parameters that must be adjusted according to a chosen criteria function using a learning algorithm. In this way, ANNs are able to capture many higher-order correlations that may exist in the data, which typically results in a nonlinear map.

The back-propagation algorithm is used to train the network with the data [10]. The training process determines the weights of ANNs to fit a suitable nonlinear map. The back-propagation's effectiveness in training an ANN often results in better modeling than does linear regression, but this method has several weaknesses. The back-propagation algorithm is based on local descent and can get stuck in different local minima based on the starting weights; as a

result, the predictive properties of resultant ANNs can be quite varied. Also, there are a number of tunable parameters such as starting weights and learning rates that have a significant effect on the final weights computed by the back-propagation algorithm. Thus, when different ANN models are trained with the same back-propagation algorithm but with different starting weights and learning rates, the performance can be significantly different. But since each such neural network achieves local minimum, it performs the best for that locality; and the projective fusers ensure that such local optimality is preserved [8]. Six independent variables-Cu, Ni, P, fluence, irradiation temperature, and effective full-power time-were used in the ANN models.

K-nearest-neighbor regression (K-NNR) method. The NNR [9] is also chosen to generate an embrittlement model because it is non-smooth and hence is qualitatively dissimilar to smooth ANNs. Typically, disparate models result in better fuser performance. The algorithm is described follows. Let x_1, $x_2, x_3, \ldots, x_n$ be a sequence of n independent measurements with known classifications, and x be the measurement to be classified. Among $x_1, x_2, x_3, \ldots, x_n$, let the measurement with the smallest distance from x be denoted as x'. Then the nearest-neighbor decision rule assigns the classification of x' to that of x. As for K-NNR, it assigns to an unclassified sample point the class most heavily represented among its K-nearest-neighbors to x. In this study, we chose the first three nearest-neighbors with properly weighted functions to represent the unclassified sample.

Six independent variables-Cu, Ni, P, fluence, irradiation temperature, and effective full-power time-were used in the K-NNR models. For the BWR data sample, a second test K-NNR model, excluding irradiation temperature from the fitting parameter, generated a trend curve nearly identical to that with irradiation temperature.

2.4. Fusion of embrittlement models

Our approach consists of identifying the error profiles of various estimators and the physical parameters of the underlying problem and designing the fusers for combining the individual estimators. Two types of information fusers were used here: the linear fuser and the nearest-neighbor projective fuser.

Initially we combined the statistical and domain-mechanism estimators using the linear fuser, which is a special case of the isolation fusers [7]. Given n estimators, $f_1(x), \ldots, f_n(x)$, the linear fuser is given by $f(x) = w_1 f_1(x) + \cdots + w_n f_n(x)$, where $w_1, \ldots, w_n$ are the weights. We computed the weights for the fuser by minimizing the error of the fuser for the training set. The program was written in C, where the solution is based on a quadratic programming problem.

The projective fuser [8] based on the nearest-neighbor concept was also implemented in the study. This fuser partitions the space of domain X into multiple regions based on the nearest-neighbor to the sample. For each region an estimator with the lowest empirical error is used to compute the function estimate for all points in the region. This fuser is easy to implement and provides finite-sample performance bounds under fairly general smoothness or non-smoothness conditions on the individual estimator.

In this study, we utilized the linear fuser and the nearest-neighbor projective fuser to develop the embrittlement models. Six parameters-Cu, Ni, P, fast fluence, irradiation time, and irradiation temperature-were incorporated into model development. Eight different models were investigated, including four neural network models, two WRK models (excluding the baseline model), the K-NNR method, and the Eason model.

WRK Fuser Model I. Linear fuser was implemented into Fuser Model I development. The results of the linear fuser model indicate that this newly developed embrittlement model achieves significant reductions in uncertainties (as shown in Table 1), compared with the model of RG1.99/R2. The residual is defined as 'measured shift minus predicted shift'. The residuals and its two-sigma uncertainties for the combined PWR and BWR data are illustrated in Figs. 1 and 2 for base and weld materials, respectively. The weights of WRK Fuser Model I are listed in Table 2, and the associated one standard deviation for training set and test set data are stated in Table 3.

WRK Fuser Model II. The nearest-neighbor projective fuser was implemented in Fuser Model II development. The results of the projective fuser model indicate that significant reductions in uncertainties were achieved, as shown in Table 4, compared with the results of RG1.99/R2. The residual and its two-sigma uncertainties for the combined PWR and BWR data are illustrated in Figs. 3 and 4 for base and weld materials, respectively.

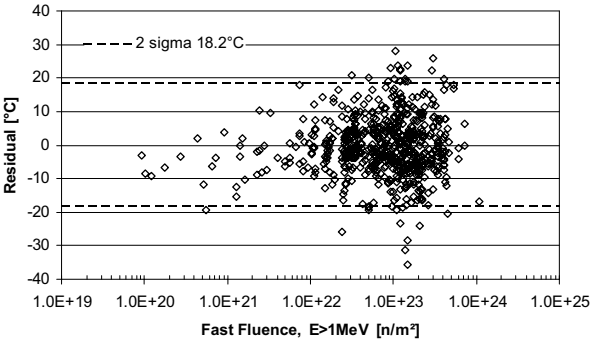

Fig. 1. Linear fuser model's residual for PWR + BWR base data, with 2-sigma uncertainty of 18.2 °C.

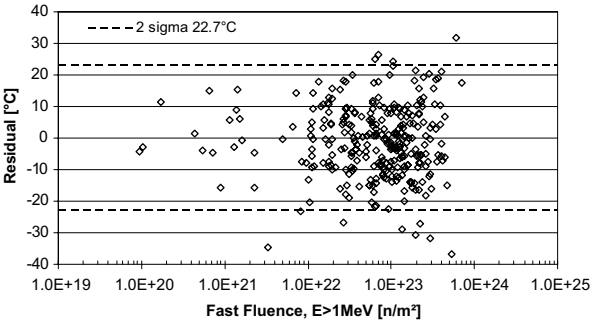

Fig. 2. Linear fuser model's residual for PWR + BWR weld data, with 2-sigma uncertainty of 22.7 °C.

A few modifications were made to make the K-NNR fuser and the nearest-neighbor projective fuser more robust. Neutron fluence is measured in units of 10^{19} n/cm^2, which leads to a small squared error, and this results in less contribution from fluence data in fuser model development. Hence, there is a need to scale this variable in such a way that it makes a contribution that is equal or comparable to that of the other variables in the model formulation. The fluence was multiplied by 10 times to increase its contribution to be on a par with that of copper and of nickel. The code was edited accordingly, and the results were derived.

A few more alterations to the extent of fluence contribution were investigated. This was done for the weld data and the nearest-neighbor projective fuser model. The fluence was weighted with a factor 5, 3, or 1 instead of 10, which is in accordance with engineering judgment. The prediction of the higher fluence points seem to perform better with the lower weight factor. The contribution of higher fluence points to fuser model development is significant, even without the factor 10. Hence, the range of the high fluence and low fluence is very critical to model development similar to the case of copper content.

Also, the nearest-neighbor projective fuser test data relies entirely on one value of the least sum of squared error. To make the model more stable and capture all the points nearest to the test data, the algorithm was modified to include the nearest three neighbors to the test data. This methodology can be more stable when the data set is large and covers the entire range of variable values.

Table 3
One standard deviation of residuals for WRK Fuser Model I

Data type	One standard deviation of residuals °C (°F)			
	Base		Weld	
	Training set/point	Testing set/point	Training set/point	Testing set/point
BWR	11.6(6.4)/73	12.0(6.7)/10	15.6(8.7)/60	23.1(12.8)/9
PWR	16.1(8.9)/468	24.3(13.5)/50	20.0(11.1)/208	20.4(11.3)/20
BWR + PWR	15.1(8.4)/541	25.0(13.9)/60	20.0(11.1)/268	24.4(13.6)/30

Table 4
Two-sigma uncertainty bound of residual for WRK Fuser Model II and the RG1.99/R2's model

Data type	Residual uncertainty °C (°F)				Reduction in uncertainty from Fuser Model II (%)	
	RG 1.99/R2 Model		WRK Fuser Model I			
	Base	Weld	Base	Weld	Base	Weld
BWR	27.5(49.6)	33.0(59.4)	9.3(16.8)	11.8(21.2)	66.1	64.3
PWR	26.7(48.2)	33.8(60.8)	13.9(25.1)	14.3(25.7)	47.9	58.3
BWR + PWR	27.0(48.6)	34.9(62.8)	13.7(24.6)	16.7(30.1)	49.4	52.1

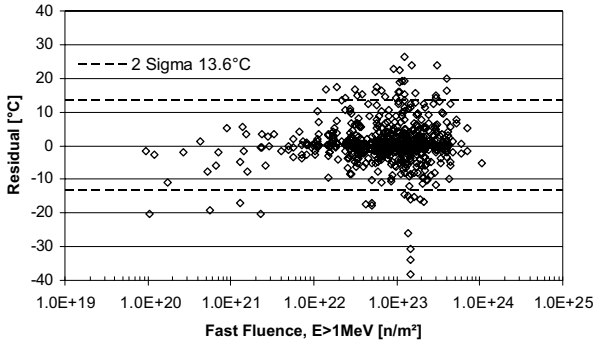

Fig. 3. KNN-fser model's residual for PWR + BWR base data, with 2-sigma uncertainty of 13.6 °C.

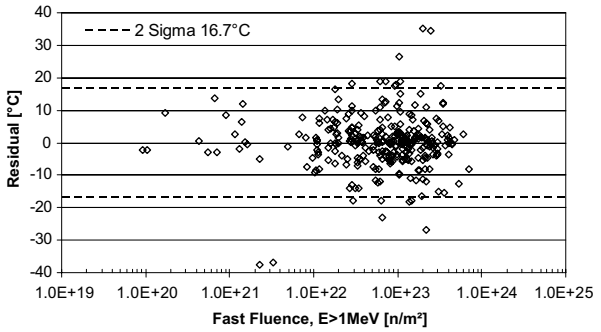

Fig. 4. KNN-fuser model's residual for PWR + BWR weld data, with 2-sigma uncertainty of 16.7 °C.

3. Discussion

A comparison of the performance of the embrittlement models, based on the two-sigma uncertainty of residual values, is shown in Tables 5–7. The Fuser Model II gave the best performance among all the embrittlement prediction models for three sample spaces: the BWR, PWR, and combined BWR and PWR data. Based on the residual for PWR or combined PWR and BWR data, the WRK Model II is marginally better than Model I, while Model III shows a relative large improvement over Model II. However, the earlier study for BWR data [1], indicates that the embrittlement model with an irradiation-time parameter does generate a much smaller 2-sigma uncertainty compared to uncertainty without the irradiation-time parameter in the embrittlement model. Furthermore, because of the marginal improvement in the uncertainty achieved from WRK Model II as compared to WRK Model I for BWR data, the embrittlement model for the BWR data is less dependent on the irradiation temperature. Fusion modeling based on BWR data provides the best performance. This superior prediction may be partially due to the small subset of power reactor data used in model development. However, by the same token, this study may also demonstrate the superiority and advantage of using subset data-for example, vendor-specific data-to develop power reactor embrittlement models. In general a large data set with similar characteristics or controllable parameters will generate a better trend prediction than its subsets. But a misleading trend curve can result from a large data set built upon different bases and with uncontrollable parameters as revealed by its large uncertainty.

The WRK models indicate that PWR data are less sensitive to the neutron flux or dose-rate effects than are BWR data. In order to investigate this issue and the associated neutron flux population and its impact on RPV embrittlement modeling, we generated a flux distribution plot, as shown in Fig. 5.

The flux distribution plot indicates that the BWR data has very wide range of flux values, ranging

Table 5
Two-sigma uncertainty of the embrittlement models for PWR data

Embrittlement model	Variables considered						Two sigma of residuals °C (°F)	
	Cu	Ni	P	Φt	t_i	T_c	Base (518 points)	Weld (228 points)
R.G. Guide 1.99/R2	X	X		X			26.8(48.2)	33.8(60.8)
WRK Fuser Model I	X	X	X	X	X	X	19.1(34.4)	22.3(40.2)
WRK Fuser Model II	X	X	X	X	X	X	13.9(25.1)	14.3(25.7)
WRK Model I	X	X	X	X			25.4(45.8)	30.5(54.9)
WRK Model II	X	X	X	X	X		24.1(43.4)	30.4(54.7)
WRK Model III	X	X	X	X	X	X	22.5(40.5)	27.3(49.2)
Eason's Model	X	X	X	X	X	X	24.4(44.0)	29.1(52.3)
K-NNR Model	X	X	X	X	X	X	20.2(36.3)	26.6(47.9)
ANN-4 Model	X	X	X	X	X	X	46.1(83.0)[a]	55.3(99.6)[a]

[a] |Residuals| > 100 °F are not included in two-sigma uncertainty evaluation.

Table 6
Two-sigma uncertainty of the embrittlement models for combined BWR and PWR data

Embrittlement model	Variables considered						Two sigma of residuals °C (°F)	
	Cu	Ni	P	Φt	t_i	T_c	Base (601 points)	Weld (298 points)
R.G. Guide 1.99/R2	X	X		X			27.0(48.6)	34.9(62.8)
WRK Fuser Model I	X	X	X	X	X	X	18.2(32.7)	22.7(40.9)
WRK Fuser Model II	X	X	X	X	X	X	13.7(24.6)	16.7(30.1)
WRK Model I	X	X	X	X			25.2(45.3)	31.1(55.9)
WRK Model II	X	X	X	X	X		24.1(43.4)	30.9(55.6)
WRK Model III	X	X	X	X	X	X	22.4(40.3)	28.2(50.8)
Eason's Model	X	X	X	X	X	X	24.0(43.2)	30.6(55.1)
K-NNR Model	X	X	X	X	X	X	18.8(33.9)	26.2(47.2)
ANN-4 Model	X	X	X	X	X	X	46.3(83.3)[a]	55.1(99.1)[a]

[a] |Residuals| > 100 °F are not included in two-sigma uncertainty evaluation.

Table 7
Two-sigma uncertainty of the embrittlement models for BWR data

Embrittlement model	Variables considered						Two sigma of residuals °C (°F)	
	Cu	Ni	P	Φt	t_i	T_c	Base (83 points)	Weld (69 points)
R.G. Guide 1.99/R2	X	X		X			27.6(49.6)	33.0(59.4)
WRK Fuser Model I	X	X	X	X	X	X	13.0(23.4)	18.8(33.9)
WRK Fuser Model II	X	X	X	X	X	X	9.3(16.8)	11.8(21.2)
WRK Model I	X	X	X	X	X		14.5(26.1)	24.1(43.4)
WRK Model II	X	X	X	X	X	X	14.2(25.5)	23.2(41.7)
Eason's Model	X	X	X	X	X	X	20.7(37.2)	30.8(55.5)
K-NNR Model	X	X	X	X	X	X	16.4(29.6)	22.3(40.2)
ANN-4 Model	X	X	X	X	X	X	33.2(59.7)[a]	53.4(96.1)[a]

[a] |Residual| > 100 °F are not included in two-sigma uncertainty evaluation.

from 2×10^{12} to 2×10^{16} n/m^{2}s. Conversely, the PWR data has a relatively narrow band of flux, ranging from 8×10^{13} to 4×10^{15} n/m^{2}s. Thus, for a flux less than 8×10^{13} n/m^{2}s, the BWR data will be the dominated factor since there is no PWR data available. By the same token, the PWR data will be the dominant factor for a flux between 8×10^{13} to 4×10^{15} n/m^{2}s. Furthermore, due to narrow band of flux distribution for the PWR data, it will be difficult to observe the dose-rate dependence of the PWR data as compared to that of BWR data.

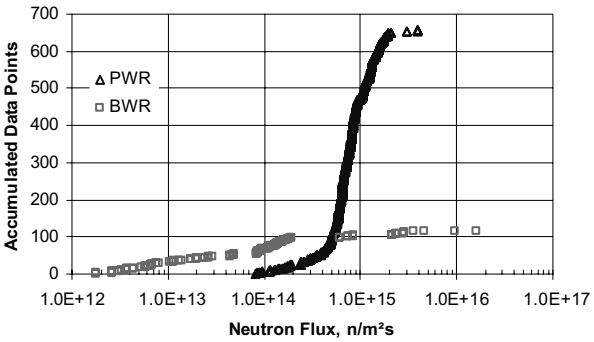

Fig. 5. Neutron flux distribution curves for PWR and BWR surveillance data, where BWR data show much wider neutron flux spectrum compared to that of PWR data.

In comparing the flux effect or the rate effect, we should not neglect the neutron energy spectrum effect. Past studies have demonstrated that a higher thermal to fast neutron ratio may have an effect on the radiation embrittlement [22–25]. For example, the BWR has a relatively soft neutron spectrum compared to that of the PWR, with the possible consequence that their respective ratios of radiation damage to fast fluence will not scale similarly. This implies that it may not be proper to combine irradiation data from different sources for modeling if their neutron spectra are not sufficiently similar. In reality, it is difficult to separate the flux and spectrum effects. However, by properly grouping the data with similar energy spectra, we may isolate the bias from a spectrum effect and gain confidence in modeling the flux effect independently. Further-

more, the benefit of separating BWR and PWR data in embrittlement modeling was clearly demonstrated from this study.

For PWR or combined PWR and BWR data, the residuals listed in Tables 5 and 6 indicate that RG1.99/R2 provides good predictions of RPV embrittlement and is compatible with WRK Model I, WRK Model II, and Eason's model. RG1.99/R2 was formulated on the basis of Guthrie's and Odette's models, and no temperature effect was considered in the embrittlement model development. The fluence factor (FF) and the plates' chemistry factor (CF) are from Guthrie's model [20]. Although total of 177 surveillance data points were used in Guthrie's model development, only 6 data points are from a BWR environment. Thus, BWR surveillance data may not be properly characterized by the RG1.99/R2 model. Furthermore, according to the PR-EDB database, the mean temperature and one standard deviation of BWR and PWR data are 279.4 ± 5.7 °C (534.9 ± 10.2 °F) and 285.6 ± 5.6 °C (546.1 ± 10.15 °F), respectively. Thus, in terms of irradiation temperatures, a bias of 6.25 °C (11.25 °F) exists between the sample temperature environments of PWRs and BWRs. There were four major commercial power reactor vendors in the United States: Westinghouse, General Electric, Babcock & Wilcox (B&W), and Combustion Engineering. Each vendor has its unique designs and specific operating procedures. There are significant problems associated with insufficient information such as the irradiation temperatures of surveillance specimens and the thermal gradients within surveillance capsules, and insufficient data about particular regions of interest to characterize the vendor's service environments. About 61% of PR-EDB data is from Westinghouse. Thus, the trend curve based on all four vendors' data will closely resemble the Westinghouse reactor environment. Furthermore, B&W surveillance data appear to show higher irradiation temperatures (based on capsule melt wire data) than data from the other vendors. Combining low- and high-temperature data may further obscure the actual bias in both data sets. For example, from the trend curve of all vendor data, the high-irradiation-temperature data shows a negative bias (i.e., a prediction model shows over-prediction), and low-irradiation temperature data show a positive bias. However, the overall biases (or uncertainties) will cancel each other, resulting in misleading statistical measures such as mean values and uncertainty.

Eason's model covers both PWR and BWR environments, in this case 96 BWR data points were included in model development, and coolant inlet temperatures were incorporated into governing equations to account for temperature effects. In practice, the coolant inlet temperature is incorporated into the embrittlement model to simulate the irradiation temperature for a pressurized light-water reactor. However, a past study [12] showed that a large bias can still be identified in Eason's model for surveillance data from a higher-irradiation-temperature environment and that the bias is similar to that of RG1.99/R2 [20]. This may indicate that the coolant inlet temperature is not a proper index to project the irradiation temperature experienced by the surveillance specimens. Furthermore, based on this study for BWR data on WRK Model I and II, neither including nor excluding coolant inlet temperature has a significant impact on the trend curve, a finding that may further support the above statement. However, for PWR data or combined PWR and BWR data, the WRK Model III shows relatively large improvement compared to WRK Model II, which may indicate that PWR data are more sensitive to the irradiation temperature parameter than BWR data, due to different ranges of irradiation temperatures.

For surveillance data, significant deviations of the measured shift from the trend curve (i.e., more or less than 18.9 °C (34 °F) for plate materials based on two sigma of RG1.99/R2 prediction for base metals) should be considered a warning flag pointing to a possible anomalous capsule environment. The large uncertainties are the result of errors in the overall description of the environment. But, limited attention has been given to characterizing the irradiation temperature environment of the surveillance specimens. In general, the neutron environment-fluence and flux-can be determined fairly accurately; and possible effects from these sources are relatively small in a power reactor environment. However, the temperature of surveillance capsule environments still relies heavily on the measurement of the melt wires. Nevertheless, the melt wire data provide important information to support the vendor-dependent embrittlement rate, which is illustrated in the transition temperature shift plot for B&W and Westinghouse data shown in Fig. 6. In general the melt wire data of B&W surveillance capsules reveal a peak temperature range between 316 °C (600 °F) and 321 °C (610 °F), and the Westinghouse data shows temperatures around 304 °C

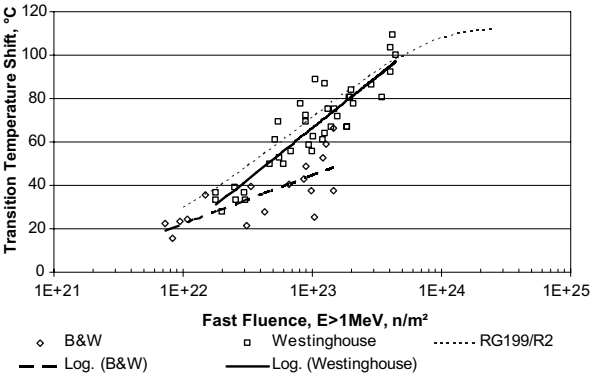

Fig. 6. Embrittlement trend curves for HSST02 material surveillance data, which indicated that B&W HSST02 embrittlement trend curve has much lower embrittlement rate compared to that of Westinghouse data.

(579 °F). In order to minimize the chemical variability from different heats, we used the standard reference material HSST02 in the study. Fig. 6 clearly indicates that B&W's data appear to be a lower bound; the B&W trend curve also shows a much lower embrittlement rate than that of Westinghouse data.

The melt wires are commonly used as a passive thermal monitor for capsules designed for RPV surveillance programs. These provide a peak temperature indication for the surveillance specimens. However, in many BWR surveillance capsules no thermal monitor was provided, and normally in the BWR surveillance reports only the reactor design operating temperature specified as 288 °C (550 °F), is provided. Therefore, a more detailed analytical investigation of specimen temperature is needed, based on detailed neutronic and thermo-mechanical analysis for specific capsule and specimen-loading configurations, to improve confidence in trend curve development. In the absence of this confirmation, the most likely reason for deviations from the trend curve is the specimen temperature.

4. Conclusions

We used the information fusion technique to obtain embrittlement predictions for the RPVs of US power reactors by combining mechanism models with neural networks and NNRs. For PWR data, our method resulted in 47.9% and 58.3% reductions in two-sigma uncertainties compared with the RG1.99/R2 model for base and weld materials, respectively. For BWR data, our method resulted in 66.1% and 64.3% reductions in two-sigma uncertainties compared with the RG1.99/R2 model for base and weld materials, respectively. This new approach combines conventional nonlinear estimators and mechanism-specific models into an integrated methodology applicable for modeling the processes of material aging. Such an approach could assist the nuclear industry with the issues of safety and lifetime extension for aging commercial nuclear power plants. By using a wide spectrum of methods, the proposed system could handle the subtle nonlinearities and imperfections in the database and serve as a benchmark for calibrating the existing mechanistic models. The predictions generated by our system have the potential for providing efficient, reliable, and fast results, and can be an essential part of the overall safety assessment of aging RPV materials.

Acknowledgements

This research is sponsored by the Laboratory Directed Research and Development Seed Money Program and the Radiation Safety Information Computational Center of Oak Ridge National Laboratory, and by the Materials Science and Engineering Division, Office of Basic Energy Sciences, of the US Department of Energy, under contract DE-AC05-00OR22725 with UT-Battelle, LLC.

References

[1] J.A. Wang, N.S. Rao, J. Nucl. Mater. 301 (2-3) (2002) 193.
[2] J.A. Wang, Embrittlement Data Base, Version 1, NUREG/CR-6506 (ORNL/TM-13327), U.S. Nuclear Regulatory Commission, August 1997.
[3] F.W. Stallmann, J.A. Wang, F.B.K. Kam, B.J. Taylor, PR-EDB: Power Reactor Embrittlement Data Base, Version 2, NUREG/CR-4816 (ORNL/TM-10328/R2), Nuclear Regulatory Commission, 1994.
[4] N.S.V. Rao, J. Franklin Inst. 336 (2) (1999) 285.
[5] N.S.V. Rao, in: A.K. Hyder (Ed.), Multisensor Fusion, Kluwer Academic Publishers, 2003.
[6] N.S.V. Rao, IEEE Transact. Pattern Anal. Mach. Intel. 23 (8) (2001) 904.
[7] N.S.V. Rao, Inform. Fusion 1 (1) (2000) 35.
[8] N.S.V. Rao, in: Proceedings of the Conference on Information Fusion, 2002.
[9] R.O. Duda, P.E. Hart, D.G. Stork, Pattern Classification, John Wiley and Sons, New York, 2001.
[10] M.H. Hassoun, Fundamentals of Artificial Neural Networks, MIT, Boston, 1995.
[11] L.K. Mansur, in: R. Gorden (Ed.), Kinetics of No homogeneous Processes, Freeman, 1987.

[12] J.A. Wang, in: Effect of Radiation on Materials: 19th International Symposium, ASTM STP 1366, ASTM, Philadelphia, March 2000, p. 59.
[13] J.A. Wang, in: Effect of Radiation on Materials, 18th International Symposium, ASTM STP 1325, March 1999, p. 525.
[14] J.A. Wang, F.B.K. Kam, F.W. Stallmann, Embrittlement Data Base (EDB) and Its Applications, Effects of Radiation on Material, vol. 17, ASTM STP 1270, August, 1996, p. 500.
[15] G.L. Guthrie, Charpy Trend Curves Based on 177 PWR Data Points, NUREG/CR-3391, U.S. Nuclear Regulatory Commission, 1983.
[16] G.R Odette, P.M. Lombrozo, J.F. Perrin, R.A. Wullaert, Physically Based Regression Correlations of Embrittlement Data From Reactor Pressure Vessel Surveillance Programs, EPRI NP-3319, Electric Power Research Institute, 1984.
[17] S.B. Fisher, J. T Buswell, A Model for PWR Pressure Vessel Embrittlement, Berkeley Nuclear Laboratories, Central Electric Generating Board, GL139PB, 1986.
[18] A.L. Lowe Jr., J.W. Pegram, Correlations for Predicting the Effects of Neutron Radiation on Linde 80 Submerged-Arc Welds, BAW-1803, Rev. 1, May 1991.
[19] C. Brillaud, F. Hedin, B. Houssin, A Comparison Between French Surveillance Program Results and Predictions of Irradiation Embrittlement, Influence of Radiation on Material Properties, ASTM STP 956, 1987, p. 420.
[20] P.N. Randall, Basis for Revision 2 of the U.S. Nuclear Regulatory Commission's Regulatory Guide 199, Radiation Embrittlement of Nuclear Reactor Pressure Vessel Steels: An International Review (Second Volume), ASTM STP 909, 1986, p. 149.
[21] E.D. Eason, J.E. Wright, G.R. Odette, Improved Embrittlement Correlations for Reactor Pressure Vessel Steels, NUREG/CR-6551, U.S. Nuclear Regulatory Commission, 2000.
[22] R.E. Stoller, L.R. Greenwood, An Evaluation of Neutron Energy Spectrum Effects in Iron Based on Molecular Dynamics Displacement Cascade Simulations, ASTM 1366, American Society for Testing and Materials, 2000, p. 548.
[23] R.E. Stoller, G.R. Odette, J. Nucl. Mater 186 (1992) 203.
[24] I. Remec, J.A. Wang, F.B.K. Kam, K. Farrell, J. Nucl. Mater. 217 (3) (1994) 258.
[25] J.A. Wang, ARN-Atucha-I Reactor Pressure-Vessel Embrittlement, ORNL/TM-2004/44, Oak Ridge National laboratory, Oak Ridge, TN, March 2004.